Hindawi
Shock and Vibration
Volume 2017, Article ID 1396567, 10 pages
https://doi.org/10.1155/2017/1396567

Research Article

Experimental and Analytical Study on the Penetration of Corundum-Rubble Concrete Subjected to Projectile Impact

Y. L. Xue,[1] D. G. Tang,[1] W. X. Chen,[1] Z. Z. Li,[1] D. P. Li,[2] and M. L. Yao[3]

[1]*State Key Laboratory of Disaster Prevention & Mitigation of Explosion & Impact, College of Defense Engineering, PLA University of Science & Technology, Nanjing, Jiangsu 210007, China*
[2]*No. 5 Air Defense Engineering Department of PLA Air Force, Nanjing, Jiangsu 211100, China*
[3]*Key Laboratory on Electromagnetic Electro-Optical Engineering, College of Field Engineering, PLA University of Science & Technology, Nanjing, Jiangsu 210007, China*

Correspondence should be addressed to D. G. Tang; tdg6206@163.com

Received 2 June 2016; Revised 17 August 2016; Accepted 20 October 2016; Published 22 January 2017

Academic Editor: Longjun Dong

A new type of composite concrete which can be called corundum-rubble concrete (CRC) was presented to improve the resistance of protective structure to the projectile impact. Comparative experiments were conducted between CRC and reinforced concrete, and a modified Taylor model was proposed to predict the penetration depth of CRC targets. Experimental results show that CRC is much higher than reinforced concrete in both strength and hardness and shows excellent resistance to the 0.125 m-diameter projectile impact. Theoretical analyses demonstrated that the modified Taylor model's predicted results were in good agreement with the measured values.

1. Introduction

Concrete is an important material which can be used to construct protective structure to resist impact by projectiles and explosive loads [1, 2]. Much work has been done to investigate the effects of concrete targets subject to projectile impact, such as Guirgis and Guirguis [3], Wang et al. [4], Yu et al. [5], Bian et al. [6], and Wen and Lan [7]. However, most of the work was conducted to predict resistance/strength of reinforced concrete targets.

The resistance features of reinforced concrete targets include AE source characteristics, the fragment-size distribution, surface characteristics, and penetration depth. Different explosion/seismic sources will lead to disparate failure characteristics [8, 9]. The reinforced concrete targets often show lack of resistance/strength to the impact of modern weapons and powerful projectiles. Hence, it is important to study on improving the resistance/strength of reinforced concrete targets and find a concrete which has ability to resist modern projectiles impact and other explosion/seismic sources.

As was pointed in the previous studies, the most important factor affecting the resistance/strength of reinforced concrete targets was the compressive strength [10, 11], and plenty of reviews such as Sun et al. [12], Dancygier et al. [13], and Tai [14] were concentrated on improving the compressive strength of concrete to enhance the resistance/strength of reinforced concrete targets.

In this paper, a new material which can be called corundum-rubble was proposed to improve the compressive strength of concrete in order to enhance the resistance/strength of reinforced concrete targets and a new type of concrete target which can be called corundum-rubble concrete target (CRC target) was designed by casting reinforced concrete together with corundum-rubble.

The corundum-rubble is a dark brown crystal. With high quality bauxite, anthracite coal, and scrap iron as the main raw material, it was smelted in the electric-arc furnace under the high temperature of 2500°C. After smelting, the main ingredient of corundum-rubble is Al_2O_3, accounting for 94% of the total. The density of corundum-rubble is 3800 kg/m^3, the elastic modulus is 400 GP$_a$, the compressive strength is over 2000 MP$_a$, and Mohs' hardness scale is 9.1 (second only to diamond) [15].

Table 1: Parameters of projectile.

l_0 (m)	d (m)	ρ_p (kg/m^3)	σ_y (MP$_a$)	σ_d (MP$_a$)	M (kg)
0.684	0.125	7850	785	980	18.29

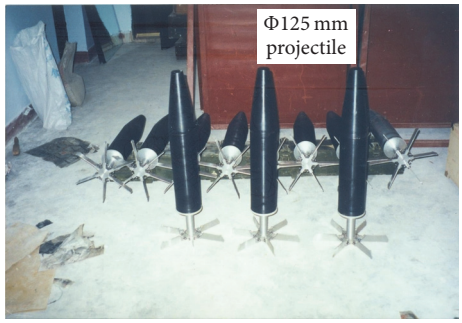

Figure 1: Projectile.

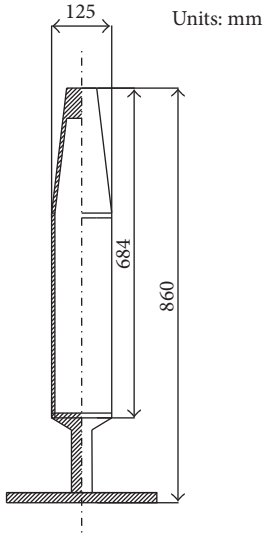

Figure 2: Structure diagram of projectile.

In this paper, comparative experiments were conducted between CRC targets and reinforced concrete targets. The experimental results were obtained to analyze the resistance/strength of CRC targets. The theoretical formulae were cited to predict the penetration depth of reinforced concrete targets and a modified Taylor model was proposed to predict the penetration depth of CRC targets.

2. Experiment

2.1. Projectile. In the experiments, a 0.684 m-length, 0.125 m-diameter, and 18.29 kg weight truncated-ogival-nosed projectile was designed and it had six empennages to control the flight stability. The projectile was machined from 40 Cr, the density is 7850 kg/m^3, the tensile strength is 980 MP$_a$, and the yield stress is 785 MP$_a$. All projectiles were quenched to enhance the strength and hardness. Figure 1 shows the formed projectiles and Figure 2 is the structure diagram of projectiles. The parameters of projectile were summarized in Table 1.

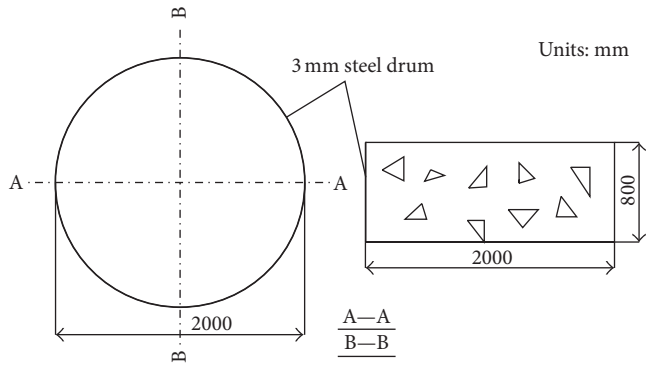

Figure 3: Diagram of reinforced concrete targets.

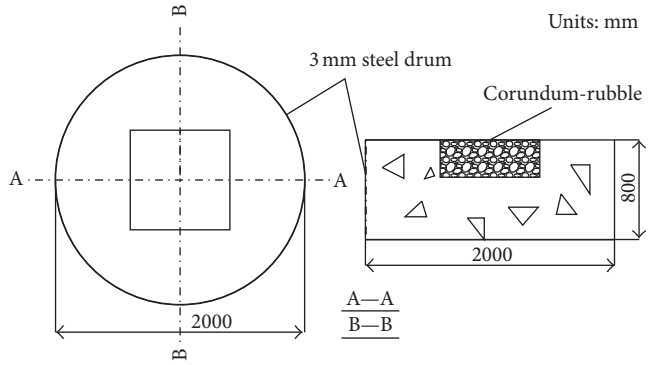

Figure 4: Diagram of CRC targets.

2.2. Targets. In the experiments, three CRC targets and reinforced concrete targets number for (N-1)~(N-3) and (C-1)~(C-3), respectively, were designed. The reinforced concrete targets were cast into 2.0 m-diameter, 0.8 m-height cylinder block and were wrapped by 0.003 m-thickness steel drums. The reinforced concrete was constructional reinforcement with Φ10 mild steel, and the area ratio of reinforcement was 0.26%. Figure 3 is the diagram of reinforced concrete targets.

CRC targets were the same size as reinforced concrete targets, which were filled with some irregular shape of 0.1~0.15 m-diameter corundum-rubble. The corundum-rubble was cast with reinforced concrete into a 0.3 m-thickness, 0.8 m-length block and located in the center of reinforced concrete targets. The reinforcement of CRC targets is the same as reinforced concrete targets and the area of reinforcement ratio is 0.26% too. Figure 4 is the diagram of CRC targets.

2.3. Experimental Method. Time measure instruments and copper mesh were used to record the initial velocity of projectiles; high speed cameras were used to capture the initial impact velocity and impact pose. A 0.125 m-diameter, smooth-bore tank gun can launch the projectiles to impact velocity of 340 m/s (or more) by changing the powder dosage. The copper mesh was 10 meters away from the tank gun. The distance from the copper mesh to the target was 25 meters. The targets faced the tank gun and were perpendicular to

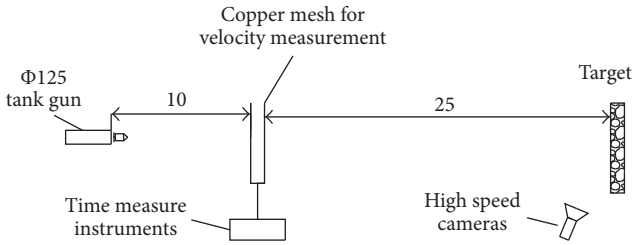

Figure 5: Experiments set-up.

the ground to make sure projectiles impact targets vertically. Figure 5 is the experiments set-up.

3. Experimental Results

3.1. The Damage of Projectiles. After impacting the reinforced concrete targets, the projectiles got slight damage and stayed with intact shape. While, after impacting the CRC targets, all projectiles got heavily damaged, none of them had the intact shape. Figures 6 and 7 are damaged projectiles of reinforced concrete targets and CRC targets, respectively.

Figure 6 shows the damaged projectiles after impacting the reinforced concrete targets. One of these three damaged projectiles with the initial velocity of 356 m/s got the most serious damage and all the empennages were broken, but the shape of projectile stayed intact. The other two projectiles also got slight damage and the shape stayed intact.

Figure 7 shows the damaged projectiles after impacting the CRC targets. These three projectiles got serious damage. When the initial velocities were 355 m/s and 356 m/s, the projectiles were severely bended in one-third of them. When the initial velocity was 353 m/s, the projectile was truncated into two pieces. Besides, all the empennages of these three projectiles were broken.

3.2. The Damage of Targets. As was shown in Figure 8(C-1), the reinforced concrete target got serious damage (both the front face and rear face subjected to projectile impact). The front face of target formed a 0.82~0.95 m-diameter, 0.603 m penetration depth crater, and there are seven obvious cracks around the target body. At the rear face, a 1.1~2 m-diameter and 0.445 m-depth cone cracking zone was formed, and the target was perforated. The similar phenomena appeared in Figure 8((C-2), (C-3)) and the detailed descriptions were summarized in Table 2.

In Figure 9(N-1), a 0.66~0.82 m-diameter and 0.18 m penetration depth crater was formed at the front face of CRC target subjected to projectile impact. It is noteworthy that the rear face stayed intact. Figure 9((N-2), (N-3)) had the similar phenomena and the detailed descriptions were summarized in Table 2 too.

From Figures 8 and 9 and Table 2, we can demonstrate that the resistances/strengths of CRC targets were much higher than reinforced concrete targets. The maximum depth of penetration of CRC targets is 0.18 m, which is 63% less than the minimum penetration depth of reinforced concrete targets.

Table 2: Experimental results.

Number	M/kg	v_0/(m/s)	h_p/m	d_c/m	d_z/m	h_z/m
(C-1)	18.7	353	0.603	0.82~0.95	1.10~2.00	0.445
(C-2)	18.6	347	0.489	0.96~1.23	1.55~1.43	0.370
(C-3)	19.5	356	0.599	0.98~1.30	1.08~1.10	0.450
(N-1)	18.9	355	0.180	0.66~0.82	/	/
(N-2)	19.2	356	0.170	0.57~0.70	/	/
(N-3)	18.5	353	0.050	0.40~0.42	/	/

4. Theoretical Analysis of Penetration Depth

4.1. Penetration Depth of the Reinforced Concrete Targets. Many empirical and semianalytical formulae were proposed to calculate penetration depth of concrete targets in recent years. Some of them were widely used in plenty of reviews such as BRL, ACE, and NDRC. Herein, we listed some formulae in the following.

4.1.1. The Modified Ballistic Research Laboratory (BRL) Formula Is Given by [3]

$$\frac{x}{d} = \frac{1.33 \times 10^{-3}}{\sqrt{f_c}} \frac{M}{d^3} d^{0.2} V_0^{1.33}. \tag{1}$$

4.1.2. The US Army Corps of Engineers (ACE) Formula Is Given by [3]

$$\frac{x}{d} = \frac{3.5 \times 10^{-4}}{\sqrt{f_c}} \frac{M}{d^3} d^{0.215} V_0^{1.5} + 0.5. \tag{2}$$

4.1.3. The Modified Formula of National Defence Research Committee (NDRC) Is Given by [3]

$$G = \frac{3.8 \times 10^{-5} N^* M}{d\sqrt{f_c}} \left(\frac{V_0}{d}\right)^{1.8}, \tag{3}$$

where function G is given by

$$G = \begin{cases} \left(\dfrac{x}{2d}\right)^2, & \text{for } \dfrac{x}{d} \le 2, \\ \dfrac{x}{d} - 1, & \text{for } \dfrac{x}{d} > 2. \end{cases} \tag{4}$$

4.1.4. The United Kingdom Atomic Energy Authority (UKAEA) Formula [3]. Based on extensive studies conducted for the penetration of nuclear power plant structures in the UK, Barr suggested the following further modification to the NDRC

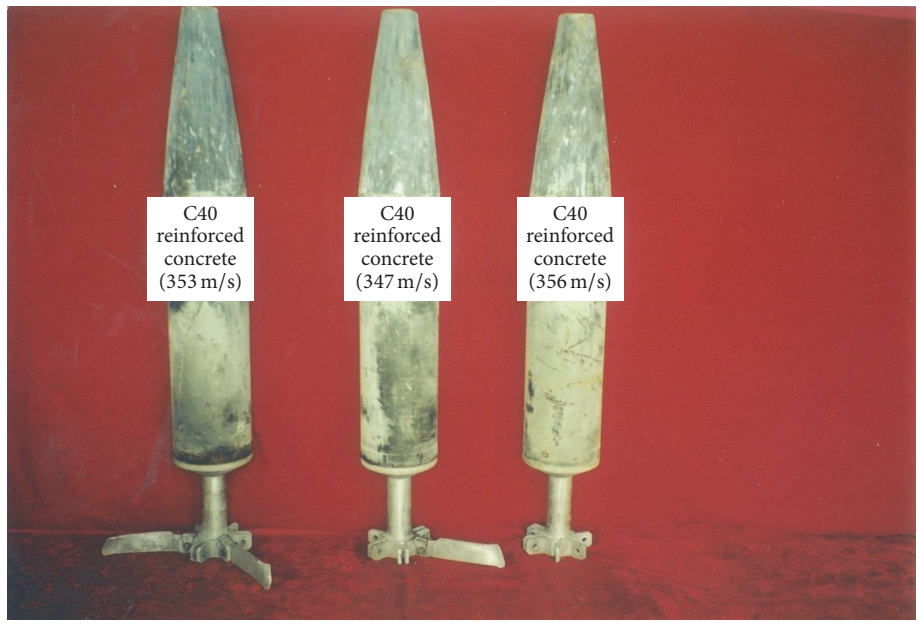

Figure 6: Damaged projectiles of reinforced concrete targets.

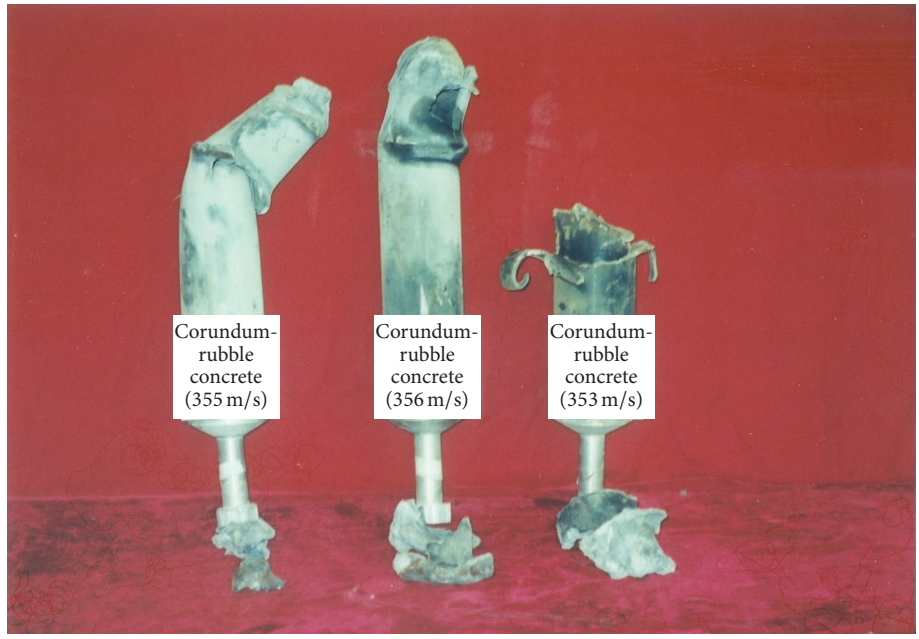

Figure 7: Damaged projectiles of CRC targets.

formula, directed mainly toward the lower impact velocities more relevant to the nuclear industry:

$$G = \frac{3.8 \times 10^{-5} N^* M}{d\sqrt{f_c}} \left(\frac{V_0}{d}\right)^{1.8}, \tag{5}$$

where function G is defined by

$$\frac{x}{d} = \begin{cases} 0.275 - [0.0756 - G]^{0.5}, & \text{for } G \le 0.0726, \\ [4G - 0.242]^{0.5}, & \text{for } 0.0726 \le G \le 1.0605, \\ G + 0.9395, & \text{for } G \ge 1.0605. \end{cases} \tag{6}$$

4.1.5. The UMIST Penetration Formula Is Given by [17, 18]

$$\frac{x}{d} = \left(\frac{2}{\pi}\right) \frac{N^* M {V_0}^2}{0.72\sigma_t d^3}, \tag{7}$$

where σ_t is defined by

$$\sigma_t \left(\mathrm{MP_a}\right) = 4.2 f_c \left(\mathrm{MP_a}\right) + 135.0 + \left(0.014 f_c \left(\mathrm{MP_a}\right) + 0.45\right) V_0. \tag{8}$$

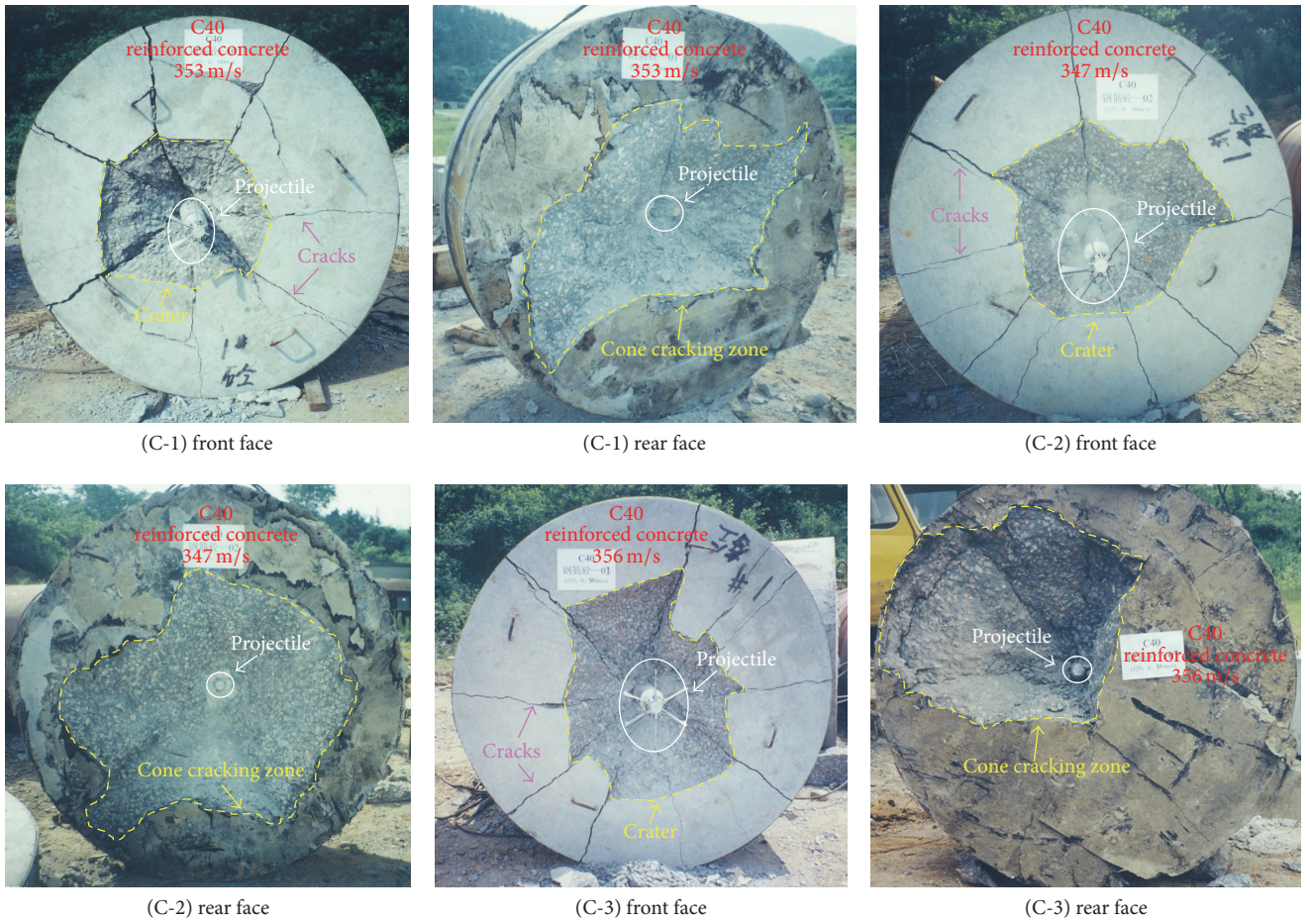

(C-1) front face (C-1) rear face (C-2) front face

(C-2) rear face (C-3) front face (C-3) rear face

Figure 8: Damage of reinforced concrete.

4.1.6. The Wen and Yang Penetration Formula Is Given by [16]

$$\frac{x}{d} = \frac{2MV_0^2}{\pi\sigma d^3}, \tag{9}$$

where σ is defined by

$$\sigma = \left(\alpha + \beta\sqrt{\frac{\rho_m}{\sigma_m}}V_0\right)\sigma_m \tag{10}$$

and σ_m is defined by

$$\sigma_m = \begin{cases} 1.4f_c + 45, & \text{for } f_c \le 75\,\text{MP}_\text{a}, \\ 150, & \text{for } 75\,\text{MP}_\text{a} \le f_c \le 150\,\text{MP}_\text{a}, \\ f_c, & \text{for } f_c \ge 150\,\text{MP}_\text{a}, \end{cases} \tag{11}$$

where α and β are given in Table 3.

In Table 4, some famous penetration formulae were quoted to calculate the penetration depth of reinforced concrete targets and the calculated results were compared with the experimental results. We can draw a conclusion that the experiments we conducted are reasonable and experimental results are reliable.

Table 3: Values of various parameters for concrete targets [16].

Shape	α	β
Conical-nosed ($\theta < 90^\circ$)	$\frac{1}{2}\left[1 + \ln\frac{2E}{(5-4\nu)\sigma_m}\right]$	$2\sin\frac{\theta}{2}$
Conical-nosed ($90^\circ \le \theta < 180^\circ$)	$\frac{1}{2}\left[1 + \ln\frac{2E}{(5-4\nu)\sigma_m}\right]$	$\sqrt{2}$
Flat-nosed	$\frac{1}{2}\left[1 + \ln\frac{2E}{(5-4\nu)\sigma_m}\right]$	$\sqrt{2}$
Ogival-nosed	$\frac{2}{3}\left[1 + \ln\frac{E}{3(1-\nu)\sigma_m}\right]$	$\frac{3}{4}\psi$
Hemispherical-nosed	$\frac{2}{3}\left[1 + \ln\frac{E}{3(1-\nu)\sigma_m}\right]$	$\frac{3}{2}$

4.2. Penetration Depth of the CRC Targets. The projectiles penetration effects researches of high strength concrete had attracted much attention. A variety of calculation models have been proposed, such as FFI model [19, 20], Riera and Iturrioz model [21], Taylor model [22], Tate model [23, 24], and Lee-Tupper model [25]. The FFI model is suitable for the 0.012 m-diameter projectile with the impact velocity from 400 m/s to 1700 m/s. Targets deformation has not been considered in both the Riera and Iturrioz model and Taylor

Table 4: Comparisons of various equations with the test data for the DOP of reinforced concrete.

Penetration formulae	(C-1)		(C-2)		(C-3)	
	x/d	x	x/d	x	x/d	x
BRL	2.967	0.371	2.873	0.359	3.129	0.391
ACE	2.551	0.319	2.480	0.310	2.666	0.333
NDRC	1.509	0.307	1.448	0.301	1.598	0.316
UKAEA	2.448	0.306	2.387	0.298	2.375	0.317
UMIST	1.628	0.203	1.572	0.196	1.719	0.215
Wen & Yang	5.558	0.695	5.335	0.667	5.921	0.740
Experiment results	4.824	0.603	3.912	0.489	4.792	0.599

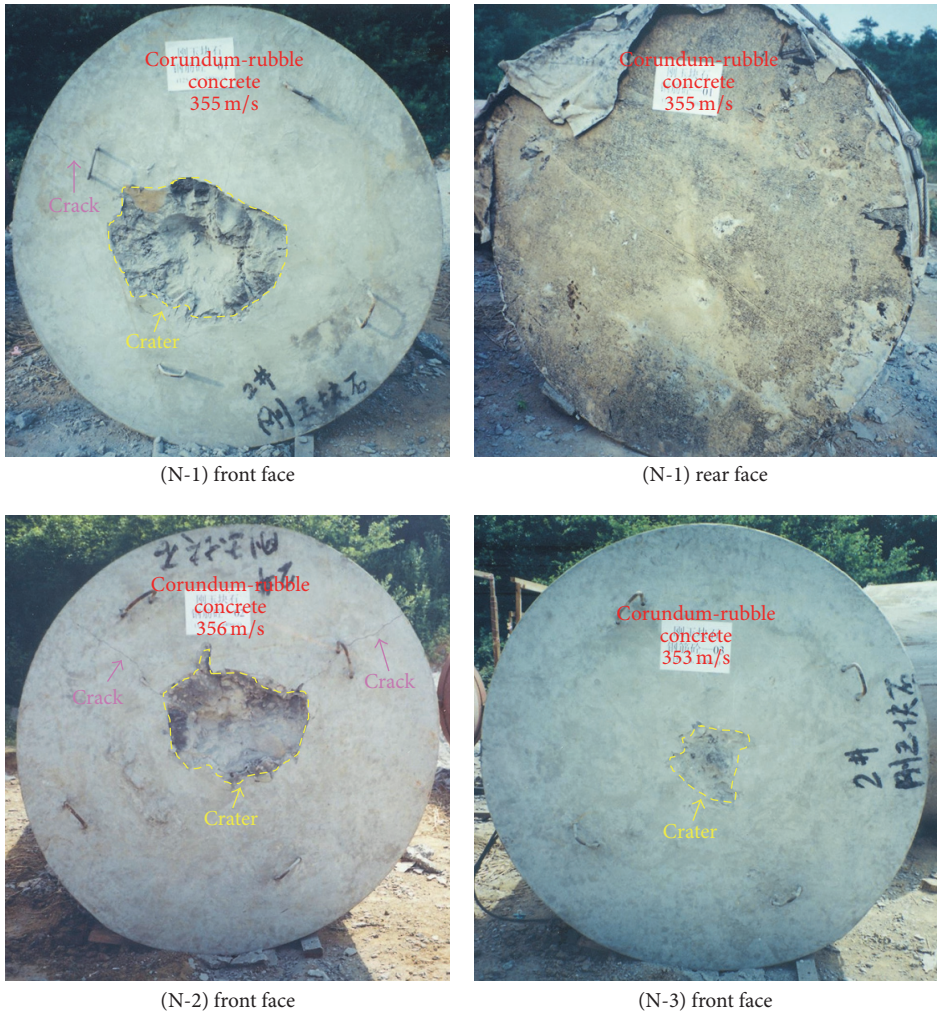

(N-1) front face (N-1) rear face

(N-2) front face (N-3) front face

Figure 9: Damage of CRC targets.

model. Riera and Iturrioz model's yield load is calculated according to pipe quasi-static axial impact load, without considering the inertia effect. It will bring a larger error to calculate the penetration depth with impact velocity above 340 m/s. Tate model focuses on the impact velocity above 1000 m/s; in this paper, the impact velocity is about 340 m/s, and the actual velocity is not more than the plastic wave velocity, so Lee-model does not suit too.

In this paper, we see the large plastic deformation as part of quality loss of projectiles. Taking targets deformation into consideration, we build a new model called "modified Taylor model" to analyze the deformation of the CRC targets.

4.2.1. Modified Taylor Model. Suppose that the projectile is flat, cylindrical, ideal rigid-plastic material, initial length is l_0, cross-sectional area is A_0, density is ρ_p, dynamic yielding

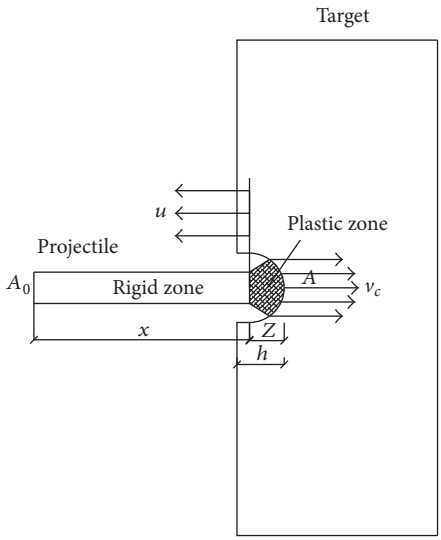

Figure 10: One-dimensional simplified diagram of modified Taylor model.

stress is σ_d, and initial velocity is v_0. The model is given in Figure 10.

In Figure 10, z is the distance between elastic-plastic interface of the projectile and projectile-target contact interface. x is the length of rigid zone, where plastic deformation has not occurred; h is the depth of penetration; u is the velocity of plastic interface, which spreads to the left; v is the velocity of rigid zone, which spreads to the front; A_0 is rigid zone section; A is the plastic zone section, which has got deformation; v_c is the anytime velocity of projectile-target contact interface, which can be deserved by the impact velocity.

In dt time, the penetration depth $dh = v_c dt$, the rigid zone length $dx = -(u + v)dt$, and the plastic zone length $dz = udt + v_c dt$; hence,

$$\begin{aligned} \frac{dz}{dt} &= u + v_c, \\ \frac{dx}{dt} &= -(u + v), \\ \frac{dh}{dt} &= v_c. \end{aligned} \tag{12}$$

The applied force of rigid zone without deformation is $\sigma_d A_0$; equation of motion is

$$\sigma_d A_0 = -\rho_p A_0 x \frac{dv}{dt}, \quad \text{where } \frac{dv}{dt} = -\frac{\sigma_d}{x\rho_p}. \tag{13}$$

According to the law of volume constancy,

$$A_0 (u + v) = A (u + v_c). \tag{14}$$

In dt time, assume that the expanding of cross-sectional area is uniform deceleration; the velocity is

$$\dot{S} = w_0 \left(1 - \frac{t}{dt}\right). \tag{15}$$

In (15), w_0 is the expanding velocity; $\dot{S}$ is the anytime cross-sectional area.

Boundary conditions are $t = 0, S = A_0, t = dt$, and $S = A$, so

$$S = (A - A_0) \left(2t - \frac{t^2}{dt}\right) + A_0. \tag{16}$$

Hence, in dt time, the momentum of plastic zone material is

$$\rho_p A_0 (u + v)\, dt \cdot v. \tag{17}$$

The momentum turns into impulse of pressure in the plastic zone, where the impulse is

$$I = \int_0^{dt} \sigma_d (S - A_0)\, dT = \frac{2}{3}\sigma_d (A - A_0)\, dt. \tag{18}$$

According to the law of conservation of momentum,

$$\rho_p A_0 (u + v)\, v = \frac{2}{3}\sigma_d (A - A_0). \tag{19}$$

Equations (12)~(19) are the control equations to analyze deformation and destruction of projectile; in these equations, variables h, x, z, v, u, and A are unknown. Initial conditions are $t = 0$, $h = 0$, $x = l_0$, $z = 0$, $v = v_0$, $A = A_1$, and $u = u_0$.

When the projectile impacts the target with a velocity of v, the contact stress of interface is σ_c, the projectile gets velocity v_1 to the left, and at the same time the target gets velocity v_2 to the right; hence, the velocity of contact interface $v_c = v_2 = v - v_1$.

According to the law of conservation of momentum, in tiny time of δt, the stress wave spreads to the left with distance of δx; hence,

$$\begin{aligned} \sigma_c \delta t &= \rho_p \delta x v_1, \\ \sigma_c \delta t &= \rho_t \delta x v_2. \end{aligned} \tag{20}$$

C_{pp} and C_{pt} were defined by the following expressions:

$$\begin{aligned} \left(\frac{\delta x}{\delta t}\right)_p &= C_{pp}, \\ \left(\frac{\delta x}{\delta t}\right)_t &= C_{pt}, \end{aligned} \tag{21}$$

where C_{pp} is the plastic velocity of projectile and C_{pt} is the plastic velocity of target.

From (20)~(21), we can deserve that

$$v_1 = \frac{\sigma_c}{\rho_p C_{pp}}, \tag{22}$$

$$v_2 = \frac{\sigma_c}{\rho_t C_{pt}}, \tag{23}$$

$$v_0 = \sigma_c \left(\frac{1}{\rho_p C_{pp}} + \frac{1}{\rho_t C_{pt}}\right). \tag{24}$$

From (22)~(24), we can deserve that

$$v_c = \frac{v}{1 + \rho_t C_{pt}/\rho_p C_{pp}}. \tag{25}$$

From (14)~(19) and the initial conditions, we can deserve that

$$\frac{3\rho_p v^2}{2K\sigma_d} = \frac{(A_1 - A_0)^2}{A_1 A_0} = \frac{A_1}{A_0} + \frac{A_0}{A_1} - 2. \tag{26}$$

In (26), $K = 1 + \rho_p C_{pp}/\rho_t C_{pt}$.

At the initial time, the initial velocity is v_0; if $\beta = 3\rho_p v_0^2/4K\sigma_d$, we can deserve the initial cross-sectional area A_1 according to (26):

$$A_1 = \left(\beta + 1 + \sqrt{\beta^2 + 2\beta}\right) A_0. \tag{27}$$

If $\alpha = \beta + 1 + \sqrt{\beta^2 + 2\beta}$, $u = u_0$, $v = v_0$, and $A = A_1$, we can deserve the velocity of plastic area u_0 and v_0 according to (14):

$$\begin{aligned} u_0 &= \frac{A_0}{A_1 - A_0} v_0 - \frac{A_1}{A_1 - A_0} v_{c0} = \frac{\alpha v_{c0} - v_0}{1 - \alpha}, \\ v_{c0} &= \frac{v_0}{1 + \rho_t C_{pt}/\rho_p C_{pp}}. \end{aligned} \tag{28}$$

To solve (25), (26), and (28), the plastic velocity of projectile C_{pp} and the plastic velocity of target C_{pt} should be determined first. We can also solve above four equations if we deserve the value of C_{pt}/C_{pp}. As we know, the plastic wave speed of projectile to target ratio is equal to 0.1, and the elastic wave speed of projectile to target ratio is equal to 0.1 too; hence, we can deserve the value of C_{pt}/C_{pp} through the value of C_{ot}/C_{op}, so the equation is given by

$$\frac{C_{pt}}{C_{pp}} = \frac{C_{ot}}{C_{op}} = \frac{\sqrt{E_{ot}/\rho_t}}{\sqrt{E_{op}/\rho_p}} = \frac{\sqrt{E_{ot}\rho_p}}{\sqrt{E_{op}\rho_t}}. \tag{29}$$

In (29), ρ_p is the density of projectile, ρ_t is the density of target, E_{op} is the elasticity modulus of projectile, and E_{ot} is the elasticity modulus of target.

Equations (12)~(19) are the differential algebraic equations, with the initial conditions of projectile and target; we can solve equations from (20) to (29) and the calculated results can be used to solve the differential algebraic equations.

Hence, the penetration depth curve is calculated as

$$\begin{aligned} h(t) = {} & -7.4 \times 10^{-9} \left(-4.49 \times 10^7 t + v_0^{1.87}\right)^{1.54} + 7.4 \\ & \times 10^{-9} \left(v_0^{1.87}\right)^{1.54}. \end{aligned} \tag{30}$$

In the experiments, (30) is the final equation to predict the depth of penetration. We can calculate the depth of penetration of different initial velocity. Figures 11(a), 11(b), and 11(c) are the depth-time curves of initial velocity, 355 m/s, 356 m/s, and 353 m/s, respectively.

Table 5: Penetration depth of experiments and equation.

Number	Initial velocity	Experimental results	Equation results
1	355	0.17	0.161
2	356	0.18	0.165
3	353	0.05	0.163

From Table 5, it is noticed that the modified Taylor model can be used to predict the penetration depths of CRC targets and would give the effective consequence.

In the experiments, the depths of penetration are 0.17 m and 0.18 m, which are consistent with the calculated results of (30), while the depth of 0.05 m is not consistent with (30)'s calculated result. It would be necessary to make an illustration that the projectile impacted the target in the vertical direction without any angle on the corundum-rubble in the experiment of initial velocity, 353 m/s. Thus, the corundum-rubble would play the most important role to resist the impact of projectile. As was shown in the front section, the compressive strength of corundum-rubble was over 2000 MP_a and Mohs' hardness scale of the corundum-rubble is 9.1, which are so high that the projectile is hardly making penetration on it, so the penetration depth is much lower than other two experimental results.

5. Conclusions

In this paper, comparative experiments were conducted to investigate the resistances/strengths and penetration depths of reinforced concrete targets and CRC targets. And the modified Taylor model was proposed to predict the penetration depths of CRC targets. From the experimental results and formulae results, we can deserve the following:

(1) The resistances/strengths of CRC targets were much higher than reinforced concrete targets, which can be validated from the damage of projectiles and targets (Figures 6, 7, 8, and 9).

(2) Through the contrastive analyses of experimental results and formulae results of penetration depth of reinforced concrete targets, we have reasons to believe that the experiments were reasonable and experimental results were credible.

(3) The penetration depth values of CRC targets validate that the modified Taylor model was available and the predicted results agreed well with the experimental results.

Notations

l_0: Length of projectile (m)
x: Penetration depth measured from the proximal face of the concrete target (m)
d: Diameter of projectile (m)
ρ_p: Density of projectile (kg/m^3)
σ_y: The yield stress of projectile (MP_a)

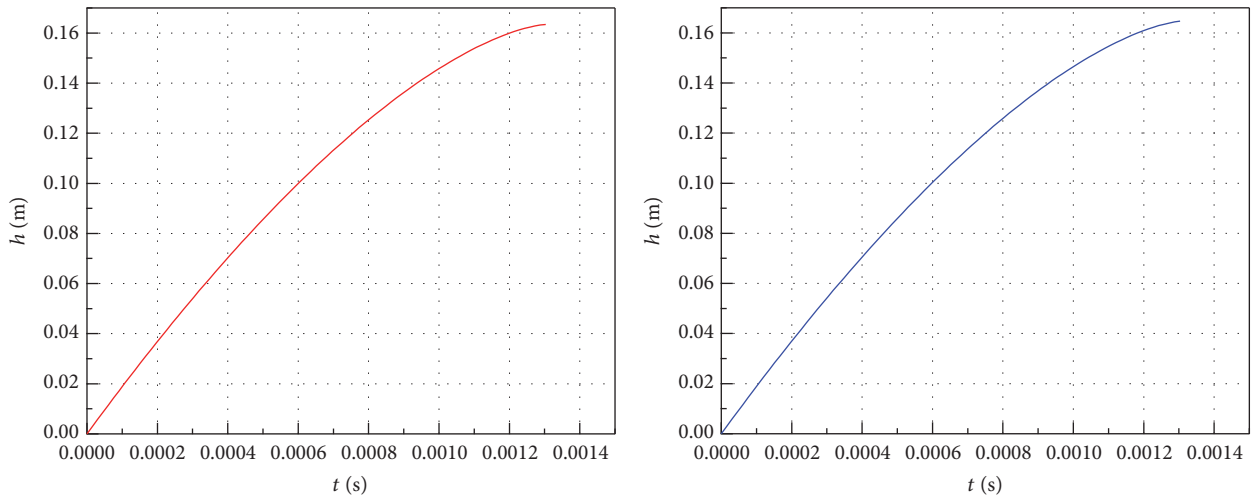

(a) Initial velocity of 355 m/s

(b) Initial velocity of 356 m/s

(c) Initial velocity of 353 m/s

Figure 11: Penetration depth curves.

σ_d: The tensile strength of projectile (MP_a)
M: Mass of the projectile (kg)
v_0: The initial velocity of projectile (m/s)
h_q: Penetration depth (m)
V_0: Projectile impacting velocity (m/s)
f_c: Unconfined compressive strength of concrete (MP_a)
N^*: Nose shape factor (N^* is a nose shape factor equal to 0.72, 0.84, 1.0, and 1.14 for flat, blunt, hemispherical, and very sharp noses, resp.)
ρ_m: Density of concrete targets (kg/m^3)
α: Constants
β: Constants
E: The modulus of elasticity of the target material
v: Poisson's ratio
θ: The cone angle of the projectile
$\psi = S/d$: The caliber-radius-head of the ogival-nosed projectile
S: The radius of the ogival nose.

Competing Interests

The authors declare that there are no competing interests regarding the publication of this paper.

Acknowledgments

The authors would like to acknowledge the National Natural Science Foundation of China (Project nos. 51578541 and 51378798) and Natural Science Foundation of Jiangsu Province (BK: 20141066) for financial support.

References

[1] H. Wang, J. Xiao, Y. Zheng, and Q. Yu, "Failure and ejection behavior of concrete materials under internal blast," *Shock and Vibration*, vol. 2016, Article ID 8409532, 7 pages, 2016.

[2] I. M. Kamal and E. M. Eltehewy, "Projectile penetration of reinforced concrete blocks: test and analysis," *Theoretical and Applied Fracture Mechanics*, vol. 60, no. 1, pp. 31–37, 2012.

[3] S. Guirgis and E. Guirguis, "An energy approach study of the penetration of concrete by rigid missiles," *Nuclear Engineering and Design*, vol. 239, no. 4, pp. 819–829, 2009.

[4] M. Wang, Z. Liu, Y. Qiu, and C. Shi, "Study on the similarity laws for local damage effects in a concrete target under the impact of projectiles," *Shock and Vibration*, vol. 2015, Article ID 585230, 16 pages, 2015.

[5] R. Yu, P. Spiesz, and H. J. H. Brouwers, "Energy absorption capacity of a sustainable Ultra-High Performance Fibre Reinforced Concrete (UHPFRC) in quasi-static mode and under high velocity projectile impact," *Cement and Concrete Composites*, vol. 68, pp. 109–122, 2016.

[6] H. B. Bian, Y. Jia, J. F. Shao, and C. Pontiroli, "Numerical study of a concrete target under the penetration of rigid projectile using an elastoplastic damage model," *Engineering Structures*, vol. 111, pp. 525–537, 2016.

[7] H.-M. Wen and B. Lan, "Analytical models for the penetration of semi-infinite targets by rigid, deformable and erosive long rods," *Acta Mechanica Sinica*, vol. 26, no. 4, pp. 573–583, 2010.

[8] L.-J. Dong, J. Wesseloo, Y. Potvin, and X.-B. Li, "Discriminant models of blasts and seismic events in mine seismology," *International Journal of Rock Mechanics & Mining Sciences*, vol. 86, pp. 282–291, 2016.

[9] L. Dong, X. Li, and G. Xie, "Nonlinear methodologies for identifying seismic event and nuclear explosion using random forest, support vector machine, and naive bayes classification," *Abstract and Applied Analysis*, vol. 2014, Article ID 459137, 8 pages, 2014.

[10] T. Elshenawy and Q. M. Li, "Influences of target strength and confinement on the penetration depth of an oil well perforator," *International Journal of Impact Engineering*, vol. 54, pp. 130–137, 2013.

[11] V. M. Gold and G. C. Vradis, "Analysis of penetration resistance of concrete," *Journal of Engineering Mechanics*, vol. 124, no. 3, pp. 328–337, 1998.

[12] Y. Y. Sun, Z. W. Yu, Z. G. Wang, and X. M. Liu, "Novel protective covering to enhance concrete resistance against projectile impact," *Construction and Building Materials*, vol. 96, pp. 484–490, 2015.

[13] A. N. Dancygier, A. Katz, D. Benamou, and D. Z. Yankelevsky, "Resistance of double-layer reinforced HPC barriers to projectile impact," *International Journal of Impact Engineering*, vol. 67, pp. 39–51, 2014.

[14] Y. S. Tai, "Flat ended projectile penetrating ultra-high strength concrete plate target," *Theoretical and Applied Fracture Mechanics*, vol. 51, no. 2, pp. 117–128, 2009.

[15] Y. Z. Tang, Corundum smelting technology. Abrasive and tools company of China, 1987.

[16] H. M. Wen and Y. Yang, "A note on the deep penetration of projectiles into concrete," *International Journal of Impact Engineering*, vol. 66, pp. 1–4, 2014.

[17] Q. M. Li, S. R. Reid, H. M. Wen, and A. R. Telford, "Local impact effects of hard missiles on concrete targets," *International Journal of Impact Engineering*, vol. 32, no. 1–4, pp. 224–284, 2006.

[18] H. M. Wen and Y. X. Xian, "A unified approach for concrete impact," *International Journal of Impact Engineering*, vol. 77, pp. 84–96, 2015.

[19] H. Sjøl and J. A. Teland, "Extension and improvement of the NDRC formula based on experiments with 12mm steel projectiles against concrete targets," in *Proceedings of the 9th International Symposium on the Interaction of the effects of Munition with Structures*, pp. 275–282, 1999.

[20] J. A. Teland and H. Sjøl, "An examination and reinterpratation of experimental data behind various empirical equations for penetration into Concrete," in *Proceedings of the 9th International Symposium on the Interaction of the Effects of Munition with Structures*, pp. 267–274, 1999.

[21] J. D. Riera and I. Iturrioz, "Discrete elements model for evaluating impact and impulsive response of reinforced concrete plates and shells subjected to impulsive loading," *Nuclear Engineering and Design*, vol. 179, no. 2, pp. 135–144, 1998.

[22] G. I. Taylor, "The use of flat-ended projectiles for determining dynamic yield stress. I. Theoretical considerations," *Proceedings of the Royal Society A: Mathematical, Physical and Engineering Sciences*, vol. 194, no. 1038, pp. 289–299, 1948.

[23] A. Tate, "Long rod penetration models—Part I. A flow field model for high speed long rod penetration," *International Journal of Mechanical Sciences*, vol. 28, no. 8, pp. 535–548, 1986.

[24] A. Tate, "Long rod penetration models—part II. Extensions to the hydrodynamic theory of penetration," *International Journal of Mechanical Sciences*, vol. 28, no. 9, pp. 599–612, 1986.

[25] E. H. Lee and S. J. Tupper, "Analysis of plastic deformation in a steel cylinder striking a rigid target," *Journal of Applied Mechanics*, vol. 21, p. 63, 1954.